phys. stat. sol. (b) **239**, No. 1, 59–70 (2003) / **DOI** 10.1002/pssb.200303239

Phenomenological theory to model leakage currents in metal–insulator–metal capacitor systems

R. Ramprasad*

Semiconductor Products Sector, Motorola, Inc. 2100 E. Elliot Road, Tempe, AZ, USA

Received 15 March 2003, revised 15 May 2003, accepted 15 June 2003
Published online 1 September 2003

PACS 73.40.Rw, 84.32.Tt

A phenomenological model intended to provide a description of leakage behavior in metal–insulator–metal (MIM) capacitor devices is presented. The model is able to predict both transient and steady state leakage currents under constant voltage bias conditions (the *J–t* characteristics), as well as *J–V* characteristics for a given voltage sweep schedule. The electronic transport processes currently implemented in the model include trap assisted tunneling (TAT) of electrons from the electrode to defect or trap states in the dielectric, modified Poole–Frenkel (MPF) emission of part of the trapped electrons to the conduction band of the dielectric, and Schottky emission of Fermi level electrons directly from the electrode to the conduction band of the dielectric. The model is able to predict many of the observed features, including characteristic slopes in *J–t* and *J–V* plots, and dependences of the leakage current on dielectric thickness, temperature and the Schottky barrier height.

© 2003 WILEY-VCH Verlag GmbH & Co. KGaA, Weinheim

1 Introduction

High dielectric constant, or high *K*, materials are becoming important due to their potential applications in embedded dynamic random access memory [1], complementary metal–oxide–semiconductor (CMOS) transistors [1], and RF capacitors [2, 3]. One of the concerns with many such high *K* materials is unacceptably high levels of leakage current. While innovative process enhancements aimed at improving the quality of the dielectric and electrode-dielectric interfaces have resulted in reduced leakage current [4, 5], the basic mechanisms underlying leakage under various experimental conditions are still unclear.

This paper addresses the leakage behavior of metal–insulator–metal (MIM) capacitor systems, with the insulating layer typically composed of a few hundred to several hundred angstroms of high *K* material. Important consequences of such thick dielectric films, in contrast to those due to $\approx$50 Å thin films typically considered in CMOS devices, are: (i) Fowler–Nordheim or direct electrode to electrode tunneling processes are relatively unimportant compared to processes related to the defect densities, (ii) time dependent or transient phenomena begin to play an important role, and (iii) defect dynamics (e.g., defect creation and migration) become important on the time scales of interest. Owing to these factors and additional complications that arise due to the large system sizes typical of MIM capacitor devices, using accurate, state-of-the-art transport methods – many of which have been developed with ultrathin dielectric layers or molecular systems in mind [6–11] – may be inappropriate. As a result, we have developed a phenomenological model that explicitly incorporates leakage current mechanisms known to be important in thick dielectric films. Furthermore, the present model is flexible enough to permit us to gradually build additional new physics into it as necessary.

* e-mail: R.Ramprasad@motorola.com

© 2003 WILEY-VCH Verlag GmbH & Co. KGaA, Weinheim

The following three main electronic processes are currently implemented in the model: (i) trap-assisted tunneling (TAT) of electrons from the electrode to unoccupied defect or trap states in the dielectric close to the electrode-dielectric interface, (ii) modified Poole–Frenkel (MPF) or internal Schottky emission of the trapped electrons from the defect levels to the conduction band of the dielectric, and (iii) Schottky or thermal-field emission of Fermi level electrons from the electrode directly to the conduction band of the dielectric. Process (i) by itself contributes to only the transient current, process (ii) to both transient and steady state currents, and process (iii) to only the steady state current. Our model can thus predict *J–t* curves under constant voltage bias conditions, and for a given *J–V* measurement schedule (amount of time spent at each voltage step), *J–V* characteristics can also be calculated. As will be seen, many observed features, including characteristic slopes in *J–t* and *J–V* plots, and dependences of the leakage current on dielectric thickness and temperature, are predicted by the model.

Each of the three processes implemented in the model involve properties intrinsic to the system. For instance, TAT is determined by the spatial and energetic distribution of trap states $N(x,E)$, the offset between the Fermi energy of the electrode and the conduction band of the dielectric, Φ_S, and the lower limit of the tunneling relaxation times, τ_0. The MPF process is determined by the mobility of electrons in the dielectric, μ, the optical part of the permittivity, ϵ_{opt}, and $N(x,E)$. Finally, the Schottky emission is determined by ϵ_{opt} and Φ_S.

Among the effects ignored in our model are field enhancement due to the roughness of the electrode-dielectric interface, trap-to-trap tunneling (TTT) of electrons from one electrode to another, and electric field assisted trap migration and generation mechanisms. Of these, the latter two are important in describing degradation and breakdown (soft and hard) phenomena.

This paper is organized as follows. The theory underlying our leakage current model is described in detail in the next section. Results using the theory are then presented in Section 3; for a uniform distribution of defect or trap states, calculated *J–t* and *J–V* characteristics are presented, followed by a discussion of the implications of non-uniform trap state distributions. We then conclude with a brief summary.

2 Derivation of leakage current expressions

The present model assumes that the total leakage current, $j_{\mathrm{tot}}(t)$, is given by: $j_{\mathrm{tot}}(t) = j_{\mathrm{TAT}}(t) + j_{\mathrm{MPF}}(t) + j_S$, where $j_{\mathrm{TAT}}(t)$ is the trap assisted tunneling current, $j_{\mathrm{MPF}}(t)$ is the modified Poole–Frenkel (MPF) emission current, and j_S is the Schottky emission current. Here, we derive the expressions for $j_{\mathrm{TAT}}(t)$ and $j_{\mathrm{MPF}}(t)$. The present derivation is based on earlier treatments of transient currents arising due to trap-assisted tunneling alone [14, 15]. Modifications implemented here include (i) inclusion of a modified Poole–Frenkel emission process, in which part of the electrons trapped due to the TAT process are lost to thermal emission to the conduction band of the dielectric, (ii) explicit time evolution of the leakage current that will help in easy inclusion of other processes, and (iii) consideration of arbitrary trap density distribution functions.

2.1 Purely trap assisted tunneling (TAT)

Assuming TAT is the only process in operation, the net rate of change of trapped electronic charge in the dielectric at each trap level is given by [14, 15]

$$\frac{\partial n(x,E,t)}{\partial t} = \left(\frac{\partial n(x,E,t)}{\partial t}\right)_{\text{metal}\rightarrow\text{dielectric}} - \left(\frac{\partial n(x,E,t)}{\partial t}\right)_{\text{dielectric}\rightarrow\text{metal}} \tag{1}$$

$$= A[N(x,E) - n(x,E,t)] - Bn(x,E,t)\,, \tag{2}$$

where $n(x,E,t)$ is the time dependent trapped electron density distribution, $N(x,E)$ is the trap distribution, and A and B are constants. $n(x,E,t)$ and $N(x,E)$ are in units of per unit volume per unit energy, and are the distribution functions in the presence of an electric field referenced to a common energy

© 2003 WILEY-VCH Verlag GmbH & Co. KGaA, Weinheim

scale; these are expressed in terms of the field-free distribution functions, n^{ff} and N^{ff}, as: $n(x,E,t) = n^{ff}(x, E + qFx, t)$ and $N(x,E) = N^{ff}(x, E + qFx)$, where x and E are respectively the spatial location away from the electrode into the dielectric and the energy level of the trap measured down from the conduction band edge of the dielectric at $x = 0$, and q and F are the electronic charge and electric field, respectively. The above partial differential equation can be solved to yield the general solution

$$n(x,E,t) = \frac{AN(x,E)}{A+B} + C\,\mathrm{e}^{-(A+B)\,t}\,. \tag{3}$$

The constant A (also called the capture constant) is given by [14–16]

$$A = f_\infty/(\tau_0\,\mathrm{e}^{2K_0x})\,, \tag{4}$$

and the constants B and C are determined using boundary conditions [14, 15]:

$$n(x,E,0) = N(x,E)\,f_0(x,E)\,, \tag{5}$$

$$n(x,E,\infty) = N(x,E)\,f_\infty(E)\,, \tag{6}$$

where f_0 and f_∞ are the Fermi functions $f_0(x,E) = \{1 + \exp\left((E + qFx - E_F)/kT\right)\}^{-1}$ and $f_\infty(E) = \{1 + \exp\left((E - E_F)/kT\right)\}^{-1}$, τ_0 is the lower limit of tunneling relaxation times (related to the electron capture cross section [16]), $K_0 = \sqrt{2m\,|E|}/\hbar$ with m, $\hbar$, k, T and E_F being, respectively, the electronic mass, Planck's constant, Boltzmann's constant, temperature and Fermi energy of the metal electrode. For the sake of brevity of expressions, the arguments of $f_0(x,E)$ and $f_\infty(E)$ will be omitted henceforth.

Substitution of A, B and C in Eq. (3) results in [14, 15]

$$n(x,E,t) = N(x,E)\left(f_\infty + (f_0 - f_\infty)\,\mathrm{e}^{-t/\tau}\right), \tag{7}$$

with $\tau = \tau_0\,\mathrm{e}^{2K_0x}$, and in a transient current density [15]

$$j_{\mathrm{TAT}}^{\mathrm{only}}(t) = q\int\limits_{x=0}^{\infty}\int\limits_{E=-\infty}^{-qFx}\frac{\partial n(x,E,t)}{\partial t}\,\frac{x}{L}\,\mathrm{d}E\,\mathrm{d}x \tag{8}$$

$$= q\int\limits_{x=0}^{\infty}\int\limits_{E=-\infty}^{-qFx} N(x,E)\,(f_\infty - f_0)\,\frac{\mathrm{e}^{-t/\tau}}{\tau}\,\frac{x}{L}\,\mathrm{d}E\,\mathrm{d}x\,, \tag{9}$$

where $j_{\mathrm{TAT}}^{\mathrm{only}}(t)$ is the current density when TAT is the only operating process, and L is the thickness of the dielectric. Note that in terms of the field free trap level distribution function, which incidentally is the input quantity rather than $N(x,E)$, $j_{\mathrm{TAT}}^{\mathrm{only}}(t)$ is given by

$$j_{\mathrm{TAT}}^{\mathrm{only}}(t) = q\int\limits_{x=0}^{\infty}\int\limits_{E=-\infty}^{-qFx} N^{ff}(x, E + qFx)\,(f_\infty - f_0)\,\frac{\mathrm{e}^{-t/\tau}}{\tau}\,\frac{x}{L}\,\mathrm{d}E\,\mathrm{d}x\,. \tag{10}$$

2.2 Incorporation of MPF process

In the present work, it is assumed that a certain fraction of the trapped electrons are lost to Poole–Frenkel emission (thermal emission of electrons from the trap states to the conduction band of the dielectric [17, 18]). The Poole–Frenkel current density is given by a simple drift equation $q\mu F\rho$, where μ and ρ are the electronic mobility in the dielectric and carrier density (per unit area of the dielectric) that participate in the Poole–Frenkel process, respectively. In standard treatments of this process, the participating carrier density is written as $\rho = \rho_0\exp\left[-(\phi_{\mathrm{PF}} - \sqrt{qF/\pi\epsilon_{\mathrm{opt}}})\,q/kT\right]$, where ρ_0 is the total

© 2003 WILEY-VCH Verlag GmbH & Co. KGaA, Weinheim

available carrier density, ϕ_{PF} is the energy difference between the conduction band edge of the dielectric and the trap level, and ϵ_{opt} is the high frequency permittivity of the dielectric. In practice, ϕ_{PF} and $K(= q\mu\rho_0)$ in the Poole–Frenkel equation, $j_{PF} = KF \exp\left[-(\phi_{PF} - \sqrt{qF/\pi\epsilon_{opt}})\, q/kT\right]$, are treated as adjustable constants, and determined by fitting to experiments [18]. This procedure implicitly assumes just one type of defect level (characterized by ϕ_{PF}). In our case, since we have a distribution of trap states, we define a modified Poole–Frenkel current density as

$$j_{MPF}(t) = q\mu F \int\limits_{x=0}^{\infty} \int\limits_{E=-\infty}^{-qFx} f_{MPF} n(x, E, t)\, dE\, dx\,, \tag{11}$$

with the Poole–Frenkel factor f_{MPF} defined as

$$f_{MPF} = \exp\left\{-\frac{q}{kT}\left(-E - \sqrt{\frac{qF}{\pi\epsilon_{opt}}}\right)\right\}. \tag{12}$$

The negative sign in front of E in the above expression is due to our convention of measuring energy with respect to the conduction band minimum of the dielectric.

Thus, at any given time, the MPF process alters the trapped distribution of electrons, which in turn alters the TAT process at subsequent times. In order to account for this, the solution outlined above for the 'TAT only' case is discretized (by discretizing the time axis), and the trapped electron density at each time step is multiplied by $(1 - f_{MPF})$, the fraction remaining after the MPF process for that time step has occured:

$$n(x, E, t_0 = 0) = N(x, E) f_0 = n'(x, E, t_0 = 0)\,, \tag{13}$$

$$j_{TAT}(t_i) = q \int\limits_{x=0}^{L} \int\limits_{E=-\infty}^{-qFx} [N(x, E) f_\infty - n'(x, E, t_{i-1})]\, \frac{e^{-(t_i - t_{i-1})/\tau}}{\tau}\, \frac{x}{L}\, dE\, dx\,, \tag{14}$$

$$n(x, E, t_i) = N(x, E) f_\infty (1 - e^{-(t_i - t_{i-1})/\tau}) + n(x, E, t_{i-1})\, e^{-(t_i - t_{i-1})/\tau}\,, \tag{15}$$

$$n'(x, E, t_i) = (1 - f_{MPF})\, n(x, E, t_i)\,, \tag{16}$$

with $N(x, E) = N^{ff}(x, E + qFx)$. It can be seen that the above set of equations reduce to Eqs. (7) and (9) when $f_{MPF} = 0$ ('TAT only' case). Thus, Eqs. (11)–(16) determine the time dependent MPF and TAT contributions to the total leakage current.

2.3 Schottky current density

Finally, the Schottky emission contribution to the total current density is given by [17–19]

$$j_S = \frac{qmk^2}{2\pi^2\hbar^3}\, T^2 \exp\left\{-\frac{q}{kT}\left(\Phi_S - \sqrt{\frac{qF}{4\pi\epsilon_{opt}}}\right)\right\}, \tag{17}$$

where Φ_S is the offset between the conduction band minimum of the dielectric and the Fermi energy of the electrode ($\Phi_S = -E_F$ according to our convention of measuring all energies relative to the conduction band minimum of the dielectric).

3 Results and discussion

3.1 Uniform distribution of trap states

We first consider the case of a uniform distribution of trap states in the dielectric: $N^{ff}(x, E) = N_0$. Unless otherwise stated, the following parameter choices – which we believe are reasonable for metal

© 2003 WILEY-VCH Verlag GmbH & Co. KGaA, Weinheim

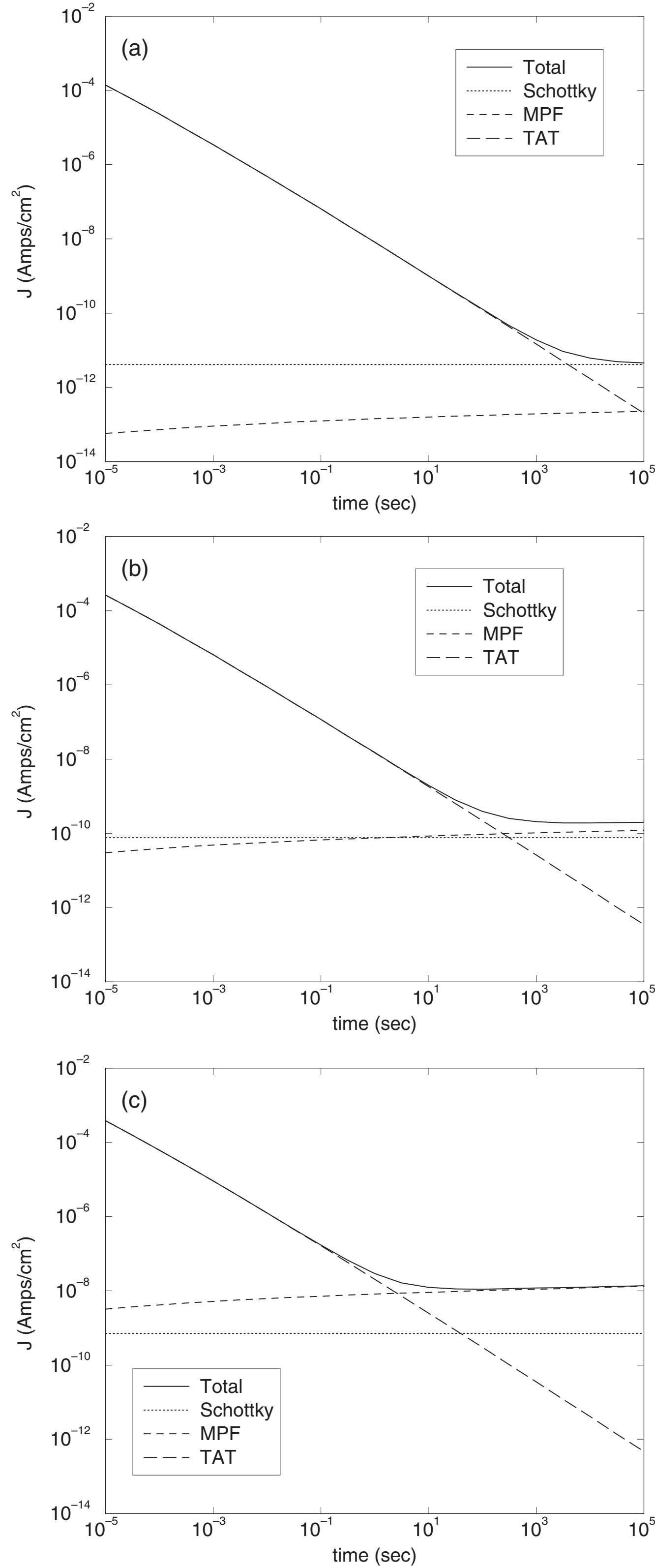

Fig. 1 J–t plots at applied voltages of a) 5 V, b) 10 V, and c) 15 V, at $T = 350$ K and $L = 400$ Å.

© 2003 WILEY-VCH Verlag GmbH & Co. KGaA, Weinheim

oxides like TaO_x – were made: $N_0 = 6.242 \times 10^{45}/(\mathrm{m}^3\ \mathrm{J}) = 1.0/(\mathrm{nm}^3\ \mathrm{eV})$, $\Phi_S = 1.5$ eV, $\epsilon_{\mathrm{opt}} = 4.0$, $\mu = 0.1\ \mathrm{m}^2/(\mathrm{V}\cdot\mathrm{sec})$, $\tau_0 = 1.0 \times 10^{-8}$ sec.

3.1.1 *J–t* characteristics

In this section, we address the scaling of the leakage current with applied voltage, temperature, thickness of the dielectric, and the barrier height.

Figure 1 shows a plot of the total leakage current as well as the three contributions to the total current as a function of time, at applied voltages of 5 V, 10 V and 15 V, at a temperature (T) of 350 K and for a dielectric thickness (L) of 400 Å. Several interesting features are apparent. Firstly, the leakage current at short times is dominated by the TAT current. It is only at longer times (depending on the applied voltage) that the MPF or the Schottky contributions take over. Secondly, the transient nature of the MPF current is evident, which increases as the TAT current decreases, with the MPF current ultimately reaching a steady state behavior. Thirdly, the slopes of the TAT contribution (and that of the total current at short times) is very close to -1 in the log–log plot. This is consistent with what is experimentally observed for numerous dielectrics, as well as for non-integrated TaO_x MIM

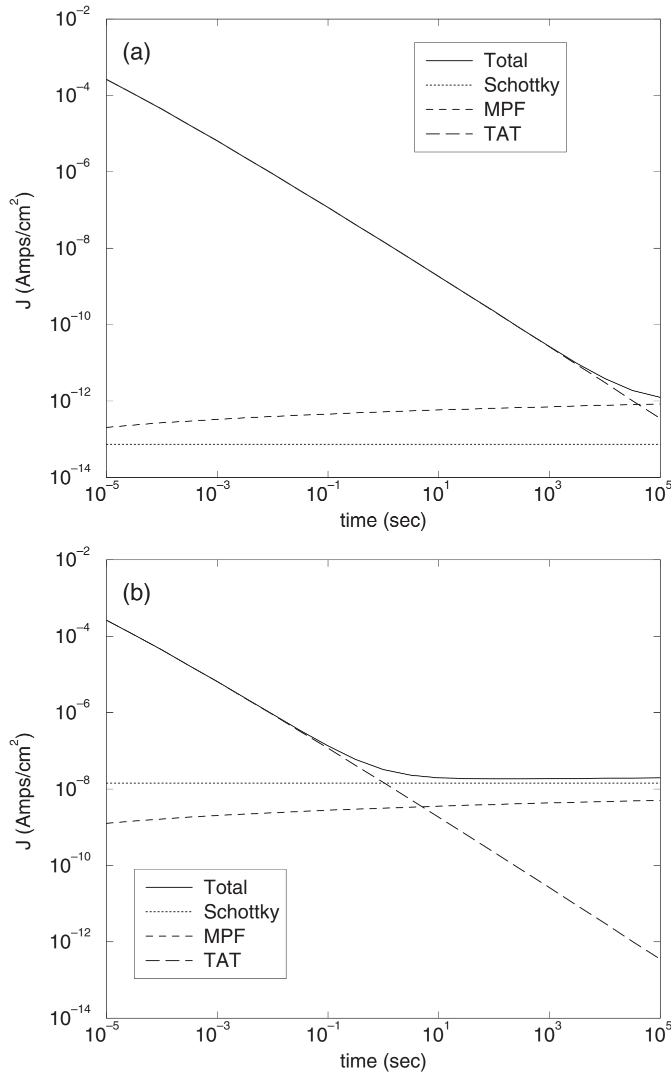

Fig. 2 *J–t* plots at temperatures of a) 300 K and b) 400 K, for $V = 10$ V and $L = 400$ Å.

© 2003 WILEY-VCH Verlag GmbH & Co. KGaA, Weinheim

capacitors [3]. Finally, the *J–t* slope of the total current in the vicinity of the transition from TAT to other processes is significantly different from −1. Thus, observed deviations of the *J–t* slope from −1 could be due to the measurement time coinciding with this transition (alternatively, such observed deviations from a slope of −1 could be due to a non-uniform distribution of defects, discussed below). It is also worth pointing out that a bulk dielectric relaxation process also exhibits transient behavior that is similar in some respects to that of the TAT process [12, 13].

Next, we consider the impact of temperature on the *J–t* behavior. Figures 2a and b show plots of *J–t* at 300 K and 400 K, respectively, for L = 400 Å and an applied voltage of 10 V; Fig. 1b shows the corresponding plot for T = 350 K. The dependence of the TAT current on temperature is much weaker than that of the other two contributions; as anticipated, the Schottky contribution has a stronger temperature dependence than the MPF current. The weak temperature dependence of the TAT current is because the temperature effects enter the TAT treatment only through the distortion of the Fermi functions, which is a weak effect. The weak temperature dependence of the transient TAT current is also consistent with short time *J–t* measurements of non-integrated TaO_x MIM capacitors [3].

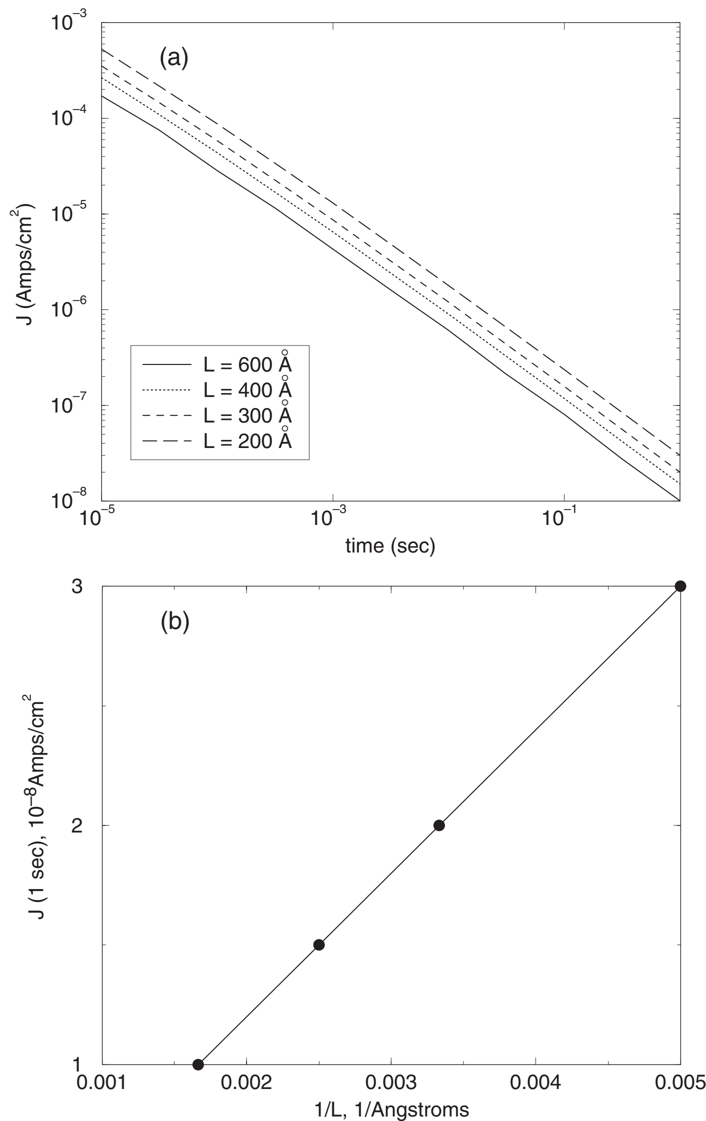

Fig. 3 a) *J–t* plots of the TAT current for various choices of the dielectric thickness (L), at a constant field of 2.5 MV/cm, and $T = 350$ K, and b) plot showing the $1/L$ dependence of the transient current.

© 2003 WILEY-VCH Verlag GmbH & Co. KGaA, Weinheim

Figure 3a shows the TAT current for various choices of dielectric thickness (L) but for a constant applied field of 2.5 MV/cm and a temperature of 350 K. In contrast to the temperature dependence seen above, the TAT current shows the largest dependence on dielectric thickness, whereas the Schottky and MPF currents show no dependence on the dielectric thickness (not shown in figure). Figure 3b shows the dielectric thickness dependence explicitly. The TAT current at 1 second is plotted against $1/L$, and the linear dependence seen is consistent with measurements of non-integrated TaO_x MIM capacitors [3].

We now attempt to assess the impact of the nature of the electrode on the leakage current. Electrodes can display varying degrees of reactivity to the dielectric, and to first order, a high reactivity electrode causes the blurring of the electrode–dielectric interface region resulting in smaller barrier heights. The higher reactivity can also cause a higher density of defects at the interface, but since we do not *a priori* know the extent of this effect, we attempt to model the reactivity by merely changing the barrier height in our simulation while holding the defect or trap density a constant. Figures 4a and b show J–t plots for barrier heights of 1.0 eV and 2.0 eV, respectively, for L = 400 Å, an applied voltage of 10 V and T = 350 K; Fig. 1b shows the corresponding plot for a barrier height of 1.5 eV.

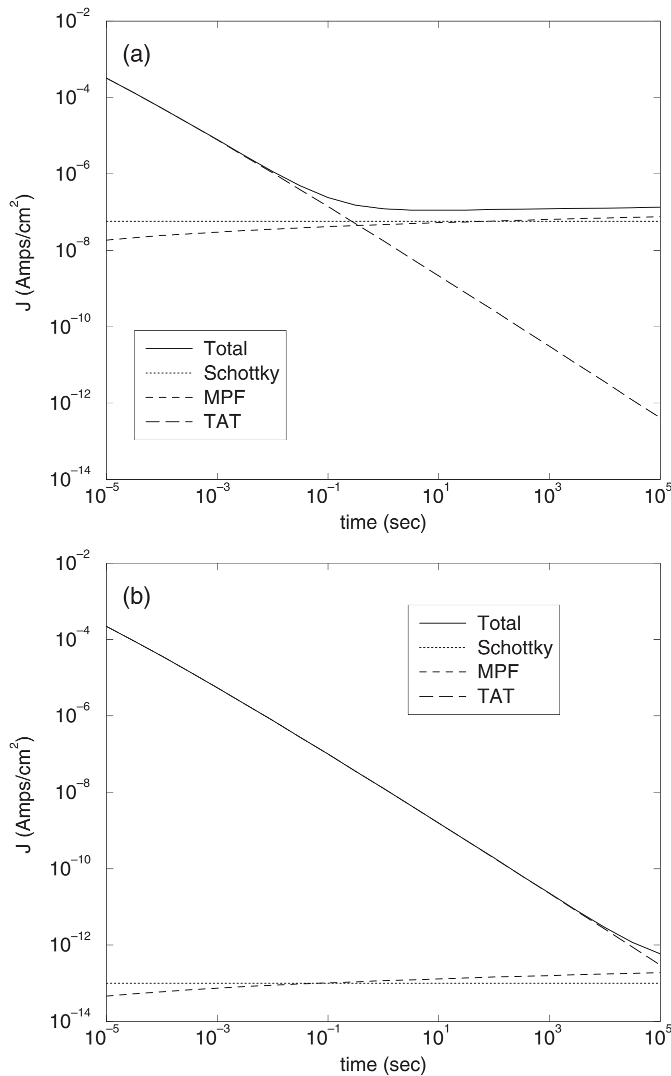

Fig. 4 J–t plots for barrier heights of a) 1.0 eV and b) 2.0 eV, for V = 10 V, $T = 350$ K and $L = 400$ Å.

© 2003 WILEY-VCH Verlag GmbH & Co. KGaA, Weinheim

Although small changes in the TAT current can be seen with changes in the barrier height, these changes are far smaller than those seen with the Schottky and MPF currents. The reason being that while the latter currents display exponential dependence on the barrier height, the TAT current for more or less homogeneous distributions of defects displays a much weaker dependence ($\approx 1/\Phi_S$) [14, 15]. Although it may be premature to conclude that the reactivity of the electrode has a minor effect on the transient current (as the impact of the electrode type on the defect distribution has been ignored in this analysis), we wish to point out that measurements on non-integrated TaO_x and HfO_2 MIM capacitors do indicate the weak dependence of the transient current on the electrode type [3].

3.1.2 *J–V* characteristics

J–V measurements involve taking current readings at predefined voltage steps, with the measurements taking longer at lower voltages than at higher voltages (the smaller magnitude of the current at lower voltages requires longer residence times for the measurement probes). As a result of this measurement procedure, the *J–t* behavior is inevitably convolved with the *J–V* characteristics. In order to facilitate a fair comparison with experiments, simulations were performed at 1 Volt steps, and the time spent at each voltage step was assumed to be 30/*V* seconds, where *V* is the applied voltage in Volts. At each voltage level, the initial electronic occupation of the trap level distribution is taken to be equal to the final occupation state at the previous voltage level.

Figure 5 shows simulated *J–V* plots at different temperatures. Several important conclusions can be drawn from these plots. First, the low voltage leakage current is dominated by the transient TAT contribution, especially at lower temperatures, with the MPF current dominating at high voltages. Second, the very prominent 'knee' feature characterized by a significant change of the *J–V* slope observed experimentally is due to a transition from TAT to MPF, and not from Schottky to Poole–Frenkel emission as is conventionally believed; the 'knee' can be seen at about 17.5 V and 12.5 V in Fig. 5a and b, respectively. The Schottky to MPF transition occurs only at high temperatures (Fig. 5c), and is characterized by a barely discernible change in slope.

3.2 Nonuniform distribution of trap states

We next consider the impact of non-uniform trap state distributions on the *J–t* characteristics. We consider a trap distribution localized in space of the form $N^{ff}(x, E) = N_0 \exp\left(-0.5((x - x_0)/x_w)^2\right)$, where x_0 and x_w are the distance from the electrode-dielectric interface and width of a gaussian spatial distribution of trap levels, respectively. N_0 and x_w are chosen to be 6.242×10^{48} and 1 Å, respectively, so that $N^{ff}(x, E)$ integrates to about 2.5 defect states per $Å^2$ per eV over the entire dielectric thickness. All other parameters were fixed at the values chosen in the previous section.

Figure 6 shows *J–t* plots of the TAT and the total leakage current for different choices of x_0, the location of the center of the gaussian distribution. An interesting feature of these plots is the flattening of the total and TAT currents at short times. The farther the defect distribution is from the interface, the longer it takes for the current to transition from the flat region. This aspect correlates with the characteristic tunneling times being longer for larger tunneling distances. It is worth mentioning that the short time *J–t* measurements on MIM capacitors do display a 'roll-off' and flattening similar to that seen in Fig. 6 [20]. Also, as mentioned earlier, deviations from a log–log *J–t* slope of -1 could arise because of non-uniform defect distributions.

The distribution of defect states that result in an observed *J–t* behavior can be simply determined by the following procedure. Arbitrary trap level distributions can be expressed as a linear combination of a number of basis functions (e.g., gaussians with varying heights and widths). The total current due to such an arbitrary distribution will be the sum of the currents due to each individual basis function. Thus, a least squares type fitting procedure can be used to determine the distribution of defect states that give rise to rich features in *J–t* curves.

© 2003 WILEY-VCH Verlag GmbH & Co. KGaA, Weinheim

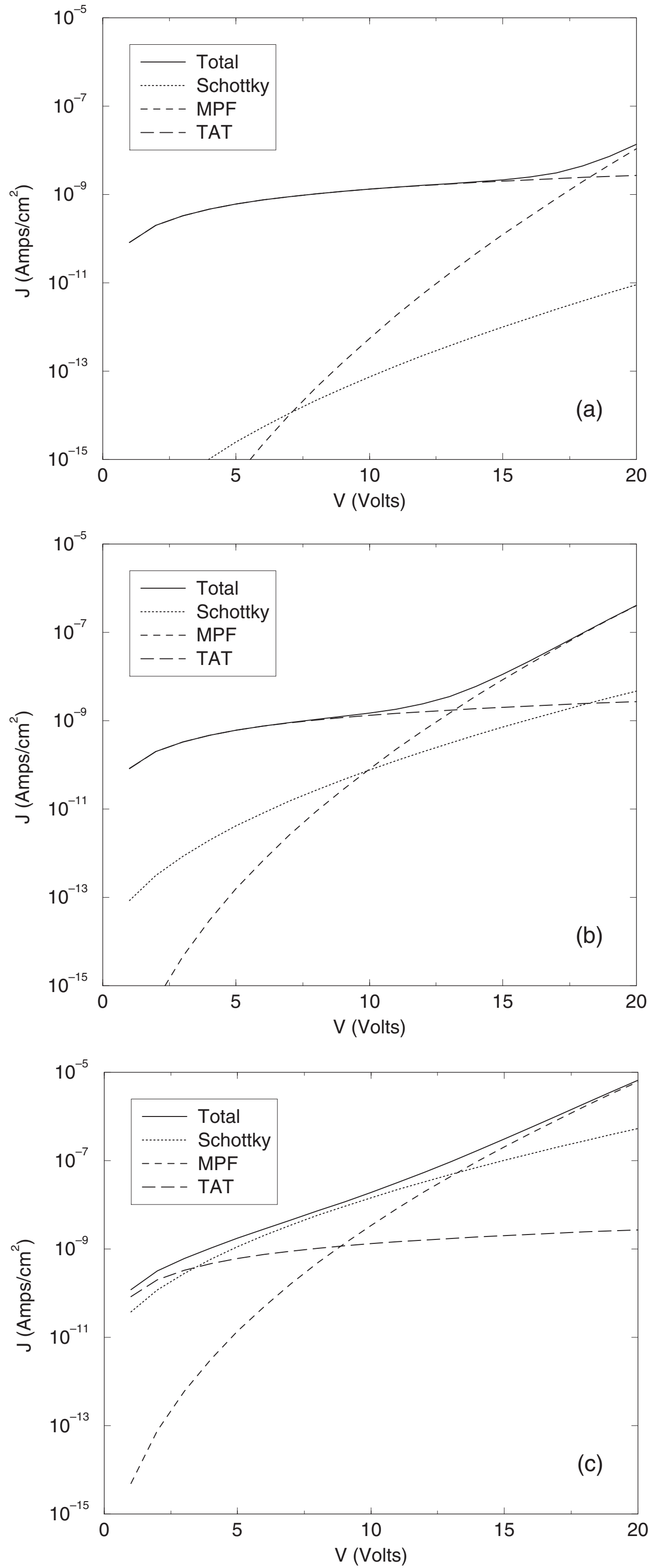

Fig. 5 J–V plots at temperatures of a) 300 K, b) 350 K and c) 400 K, for $L = 400$ Å.

© 2003 WILEY-VCH Verlag GmbH & Co. KGaA, Weinheim

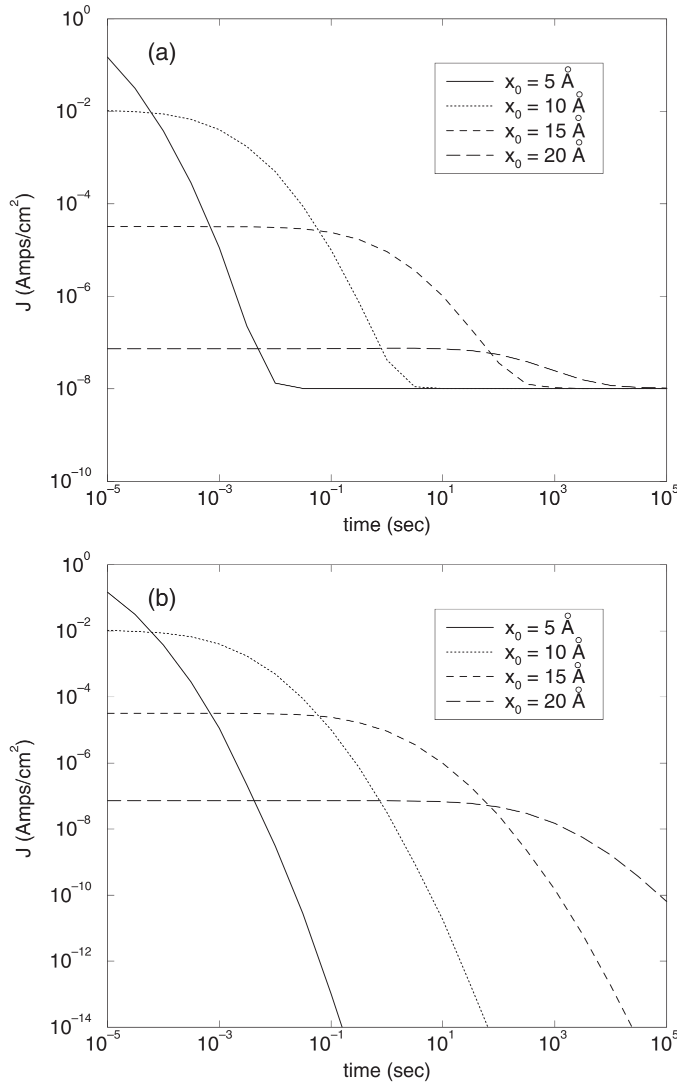

Fig. 6 *J–t* plots for a localized trap distribution, approximated by a gaussian with width 1 Å and located at a distance of x_0 from the electrode-dielectric interface at $T = 350$ K, $V = 10$ V and $L = 400$ Å: a) total leakage current and b) TAT current.

4 Summary

In summary, a model has been developed to describe the mechanisms underlying leakage currents in MIM capacitor systems. The electronic transport processes currently incorporated in the model include trap assisted tunneling (TAT), modified Poole–Frenkel (MPF) and Schottky emissions. The model is currently able to predict many of the observed features including:

1. A *J–t* slope in a log–log plot close to -1 for more or less uniform defect level distributions in the transient regime.

2. A weak temperature dependence, a 1/(dielectric thickness) dependence, and a weak dependence on the barrier height of the transient leakage current for more or less uniform defect level distributions.

3. Low field leakage dominated by TAT currents (seen in *J–V* curves), with a transition from TAT to MPF currents at higher fields.

4. Localized distributions of trap states result in a flat *J–t* response at short times, the lengths of these flat regions being longer for trap states located farther from the electrode-dielectric interface.

© 2003 WILEY-VCH Verlag GmbH & Co. KGaA, Weinheim

The model is currently unable to handle dielectric degradation and breakdown. More physics (e.g., generation and motion of defects, trap to trap tunneling, bulk dielectric effects, etc.) need to be incorporated in the model in order to provide a more complete and better description of MIM capacitor leakage *and* reliability issues.

Acknowledgements The author would like to acknowledge Tom Remmel and Mike Petras for several stimulating discussions. Mike Petras and Mel Miller are also acknowledged for critically reading the manuscript.

References

[1] Angus I. Kingon, Jon-Paul Maria, and S. K. Streiffer, Nature **406**, 1032 (2000).
[2] C. C. Barron, T. P. Remmel, D. R. Roberts, M. V. Raymond, E. D. Luckowski, S. Kalpat, M. Sadd, P. Zurcher, R. Ramprasad, and M. Miller, Proceedings of the 202nd Electrochemical Society (October, 2002).
[3] D. R. Roberts, S. Kalpat, T. P. Remmel, M. A. Sadd, M. V. Raymond, R. Ramprasad, E. D. Luckowski, and M. Miller, Proceedings of the 202nd Electrochemical Society (October, 2002).
[4] T. Remmel, R. Ramprasad, and J. Walls, to be published.
[5] G. Lucovsky, H. Niimi, Y. Wu, and H. Yang, Appl. Surf. Sci. **159–160**, 50 (2000).
[6] J. K. Tomfohr and O. F. Sankey, phys. stat. sol. (b) **226**, 115 (2001).
[7] M. Brandbyge et al., Phys. Rev. B **60**, 17064 (1999).
[8] M. P. Samanta, W. Tian, and S. Datta, Phys. Rev. B **53**, R7626 (1996).
[9] N. D. Lang, Phys. Rev. B **52**, 5335 (1995).
[10] E. G. Emberly and G. Kirczenow, Phys. Rev. B **58**, 10911 (1998).
[11] X. Zhang, L. Fonseca, and A. A. Demkov, phys. stat. sol. (b) **223**, 70 (2002).
[12] M. Schumacher and R. Waser, Integr. Ferroelectr. **22**, 109 (1998).
[13] A. Jonscher, Dielectric Relaxation in Solids (Chelsea Dielectrics Press, London, 1983).
[14] C. Cherki, R. Coelho, and R. Nannoni, phys. stat. sol. (a) **2**, 785 (1970).
[15] P. Wilcox, Can. J. Phys. **50**, 912 (1972).
[16] F. P. Heiman and G. Warfield, IEEE Trans. Electron Devices **12**, 167 (1965).
[17] S. M. Sze, Physics of Semiconductor Devices, 2nd ed. (Wiley, New York, 1981).
[18] J. J. O'Dwyer, The Theory of Electrical Conduction and Breakdown in Solid Dielectrics (Clarendon Press, Oxford, 1973).
[19] A. Modinos, Field, Thermionic, and Secondary Electron Emission Spectroscopy (Plenum Press, New York, 1984).
[20] T. Remmel, private communication (unpublished).

© 2003 WILEY-VCH Verlag GmbH & Co. KGaA, Weinheim